

Diffuse Reflection Spectroscopy: An Alternative to Autofluorescence Spectroscopy in Tongue Cancer Detection

RUPANANDA JAYACHANDRA MALLIA,* SUBHASH NARAYANAN, JAYAPRAKASH MADHAVAN, PAUL SEBASTIAN, REJNISH KUMAR, ANITHA MATHEWS, GIGI THOMAS, and JAYAKRISHNAN RADHAKRISHNAN

Biophotonics Laboratory, Centre for Earth Science Studies, Trivandrum-695031, India (R.J.M., N.S.); Department of Radiotherapy, Regional Cancer Centre, Trivandrum-695011, India (J.M.); Division of Surgical Oncology, Regional Cancer Centre, Trivandrum-695011, India (P.S.); Department of Radiation Oncology, Regional Cancer Centre, Trivandrum-695011, India (R.K.); Department of Cytopathology, Regional Cancer Centre, Trivandrum-695011, India (A.M.); and Division of Community Oncology, Regional Cancer Centre, Trivandrum-695011, India (G.T., J.R.)

Laser-induced autofluorescence (LIAF) and diffuse reflection spectroscopy (DRS) are two emerging noninvasive optical tools that have shown immense potential to detect oral cavity pre-cancer. In a recent study, we have used spectral ratio reference standards (SRRS) of LIAF intensity ratios F500/F635, F500/F685, and F500/F705 for grading of tissues belonging to sites other than dorsal side of tongue (DST), lateral side of tongue (LST), and vermilion border of lip (VBL) that exhibited similar spectral shape for normal and abnormal tissues. This led to dismal diagnostic accuracies, and for the three LIAF-SRRS, normal tissue values were often misclassified as squamous cell carcinoma (SCC), which means that the true negatives were being wrongly identified as true positives. This study examines the applicability of the site-specific diffuse reflection spectral intensity ratio (R545/R575) of the oxygenated hemoglobin bands to classify different DST lesions and compares the results obtained with those obtained using LIAF-SRRS. DRS-SRRS of R545/R575 differentiated benign hyperplastic DST tissues from normal tissue with a sensitivity of 86% and specificity of 80%, which were indistinguishable using LIAF-SRRS. Further, in distinguishing hyperplastic tissues from premalignant dysplastic lesions, DRS-SRRS gave a sensitivity of 90% and a specificity of 86%, as compared to sensitivity of 89% and specificity of 72% shown by the three LIAF-SRRS together. The diagnostic accuracy and statistical adequacy of the two techniques were assessed by receiver operating characteristic curve (ROC-Curve) analysis. Three LIAF ratios gave a low overall ROC area under curve (ROC-AUCs) of 0.521, whereas the DR ratio (R545/R575) has shown an improved accuracy of 0.970 in differentiating different tissue types. While distinguishing hyperplastic from dysplastic tissues, the DR ratio gave a higher discrimination accuracy of 0.9. Based on these findings, it can be concluded that the DRS-SRRS technique by virtue of its low cost and higher diagnostic accuracies could be a viable alternate to LIAF-SRRS for *in vivo* screening of tongue pre-cancers and grading of different tissue types.

Index Headings: Diffuse reflection spectroscopy; DRS; Laser-induced fluorescence spectroscopy; LIF; Human oral cavity; Oral/tongue cancer; Optical diagnosis of cancer; PpIX fluorescence bands; Oxygenated hemoglobin absorption bands; Receiver operating characteristic curve; ROC-curve.

INTRODUCTION

The majority of the oral cancers develop from premalignant lesions such as leukoplakia, erythroplakia, and erythroleukoplakia. The conversion rates for these incipient stages to malignant tumors are reported to be about 1–7% for homogenous leukoplakia, 4–15% for granular or verruci form leukoplakia, and 18–47% erythroleukoplakia.¹ Cancers affecting different anatomical sites of the oral cavity now account for

an estimated 274 000 new cases and 145 000 fatality cases globally each year,² and the high rates of transformation to malignancy indicate the importance and need for early diagnosis and treatment thereof. As with all cancers, early and accurate detection of neoplastic changes in the oral cavity is the preeminent method to improve the quality of life of patients, because at these embryonic stages their eradication/treatment/management measures would be much more effective. However, in usual practice, even for experienced clinicians it is not easy to distinguish visually between benign and malignant/premalignant areas within a suspicious lesion, as the severity of the lesion varies from one area to another. This, in turn, makes even the gold standard (histopathological reports of biopsy) subjective to the views of the clinician. Therefore, in order to ensure an accurate pathological diagnosis, a suspicious oral lesion may need multiple biopsies to avoid misdiagnosis of the most severe location. All these factors make the intact procedure of visual examination and ensuing biopsy-guided histopathology not only subjective, but agonizing, time consuming, and costly as well. In order to reduce patient morbidity due to the multiple biopsies, and to determine the most appropriate site for biopsy, emerging noninvasive techniques based on optical spectroscopy are showing great promise and will enable opportune diagnosis to improve patient cure and survival rates.

Various novel optical spectroscopic approaches such as laser-induced autofluorescence (LIAF), Raman, and elastic-scattering or diffuse reflection (DRS) spectroscopy have been investigated as methods for tissue discrimination by different research groups. Due to the noninvasive nature of tissue characterization these techniques are often referred to as “optical biopsies”.

Based on strong clinical rationale, many researchers have investigated the LIAF of tissues in the head and neck region and in various other organs, such as the bronchus, colon, cervix, and esophagus for developing noninvasive screening methodologies for early diagnosis of cancer.^{3–13} In LIAF, various endogenous bio-fluorophores act as sensors to provide rapid spectral information about tissue transformation.

The endogenous fluorophores that are speculated to play a vital role during carcinogenesis are amino acids, tryptophan, and tyrosine; structural proteins such as collagen and elastin; co-enzymes such as NADH and FAD; and porphyrins, and the emission from these fluorophores is strongly wavelength dependent. Carcinogenic processes produce alterations not only at the cellular level but also in the structural tissue composition, which are reflected in autofluorescence spectral

Received 25 February 2009; accepted 22 January 2010.

* Author to whom correspondence should be sent. E-mail: jrmallia@cessind.org.

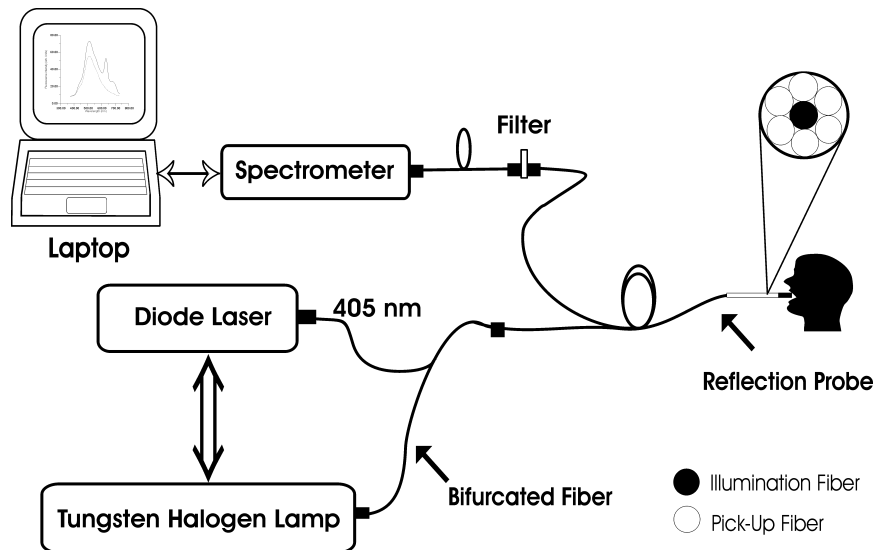


Fig. 1. Schematic of LIFRS point-monitoring system for sequential measurement of LIAF and DR spectra from the same tissue site.

line shape and intensity. Usually, alterations in the concentration of these fluorophores take place prior to major structural tissue changes, and this makes LIAF very sensitive to early tissue transformations. For example, protoporphyrin (PpIX) is an endogenous porphyrin that is associated with tissue alterations and malignancy, and it selectively accumulates in abnormal tissues due to a rupture in the heme cycle.¹⁴ Therefore, the relatively narrow fluorescence peaks from PpIX at 635 and 705 nm could provide information on the condition of mucosa under investigation.¹⁵ Conversely, the DR spectroscopic technique involves detection and analysis of a portion of the incident light that undergoes multiple elastic scattering owing to inhomogeneities in the refractive index of tissue components. Numerous optical models and systems based on this technique have shown the capability to discriminate malignancy with good sensitivity and specificity. The potential for utilizing the DR spectroscopic technique in cancer diagnosis is greater because it is cost effective and elastic interactions are much stronger than inelastic processes.

Elastic light scattering spectroscopy with polarized illumination/detection that reduces the contribution from hemoglobin absorption was used by Sokolov et al.¹⁶ to characterize *in vivo* oral cavity mucosa. Utizinger et al.¹⁷ studied the slope of reflection spectra at different source–detector separations for *in vivo* characterization of ovarian cancer and found that reflection spectral slopes between 510 and 530 nm are strongly affected by oxy- and deoxy-hemoglobin absorption and provide useful discriminatory information. The diffuse reflection spectrum has characteristic hemoglobin absorption valleys at 430, 542, and 577 nm on excitation and it is reported that hemoglobin content is more pronounced in malignant and premalignant lesions owing to increased microvasculature.¹⁸ Therefore, the oxy- and deoxy-hemoglobin bands seen in both normal and malignant tissues can be utilized to extract intrinsic tissue fluorescence that is free from artifacts induced by tissue scattering and absorption.¹⁹ Many researchers have explored the use of reflectance to correct tissue fluorescence spectral data and for understanding the effect of changes in oxygenation and tissue perfusion.^{20–23} The complementary nature of diffuse reflection and autofluorescence and their application to correct distortions

in the measured autofluorescence of oral mucosa was investigated by de Veld et al.²⁴

In a recent clinical study Rupananda et al.²⁵ has shown that spectral ratio reference standards (SRRS) derived from autofluorescence data discriminate oral cavity cancer at anatomical sites other than the dorsal side of tongue (DST), lateral side of tongue (LST), and vermilion border of lip (VBL). These three sites were excluded from the study as the healthy population spectra had spectral features similar to those of lesions. Bearing in mind the vast number of cases of tongue cancer reported in India, and the lower accuracies reported by different groups for tongue cancer detection,^{8,26,27} there exists a need to develop alternative noninvasive optical biopsy techniques to screen early stages of tongue cancer.

Subhash et al.²⁸ has for the first time proposed the use of the R545/R575 ratio of oxygenated hemoglobin absorption bands at 545 and 575 nm for grading of oral mucosa in an *ex vivo* study. This was later extended to a clinical model for diagnosing buccal lesions and in tissue grading, with the help of a spectral ratio reference standard.²⁹ This study exploits and extends the criterion based on site-specific DR spectral features of healthy tissues for detection and grading of cancer affecting DST sites. The results of the study are compared with the gold standard and with SRRS of LIAF spectral studies on the same patient cohort.

MATERIALS AND METHODS

Instrumentation. The laser-induced fluorescence and reflection spectroscopy (LIFRS) system (Fig. 1) used in this study comprises a diode laser (Model: 404 nm, 50 mW, CW; Stocker Yale Inc, Dollard-des-Ormeaux, QC, Canada) and a tungsten halogen lamp (Model LS-1; Ocean Optics, Dunedin, FL) that could be switched alternately for sequential recording of LIAF and DR spectra of tissues from the same site. A bifurcated optical fiber guides the light output from the two light sources to the oral tissue through a 3-meter-long fiber-optic probe that has a central fiber to deliver the excitation beam and six surrounding fibers (400 μm dia.) to collect LIAF/DR emission. The probe tip is terminated in a stainless steel ferrule, 15 cm long and 6 mm in diameter, to enable

sterilization before and after use. In order to provide optimum overlap between the excitation and collection areas, a black PVC sleeve (opaque) 30 mm in length was inserted at the probe tip that maintained a fixed separation of 3 mm between the probe tip and the tissue surface. This enhances the fluorescence signal and provides extra hygiene, as it can be disposed of after screening of the patient. The light emanating from the oral tissue of the patient is delivered to a miniature fiber-optic spectrometer (Model: USB 2000FL VIS-NIR Ocean Optics Inc. Dunedin, FL), connected to the USB port of a laptop computer, through optical fiber cables. During fluorescence studies, a long-wavelength pass filter (GG420; Schott Glass Technologies, Hughestown, PA) was used to block the back-scattered laser light from entering the spectrometer.

Data Acquisition and Data Processing. The laser light is focused with the optical fiber light-coupler (Model: Hydrax, Spectra Physics, CA) to project a beam with a Gaussian intensity profile onto the tissue surface. The output power at the probe tip is maintained at the same level during all measurements by monitoring with a power/energy meter (Model: PE 10-V2, Ophir Optronics, Jerusalem, Israel) before and after measurements on each subject. Slight pressure was applied with the sleeve tip of the probe on the tissue surface to prevent ambient light from entering the detection system. After each set of measurements, the probe was sterilized, and it was kept inside a plastic box. The miniature fiber-optic spectrometer was fitted with a 600 lines/mm 500 nm blazed grating for operation in the 360 to 1000 nm wavelength range. The detector used was a 2048-element linear silicon charge-coupled device (CCD) array, and in conjunction with a 200 μm slit, the monochromator produces an optical resolution of 8 nm. The LIAF and DR spectra were acquired with the help of OOI Base32 software (Ocean Optics) that was configured to record the spectra with a boxcar width of 10 nm and an integration time of 100 ms. Prior to LIAF and DR measurements, the background spectrum was recorded and the OOI Base32 software automatically subtracted the same during each measurement. LIAF and DR spectra were recorded from each mucosa/lesion in the 400–720 nm spectra window.

Study Protocol and Clinical Measurements. The clinical study included 36 healthy volunteers with no clinically observable lesions or inflammatory conditions in their oral cavity and 36 patients with measurements taken from 70 sites having clinically low-/high-risk lesions in their oral cavity. Of the aforementioned patient population, 30 sites of 16 patients were used to develop a site-specific SRRS for DST mucosa. Most of the patients studied had prolonged smoking or pan chewing habits, whereas healthy volunteers were free of such habits and maintained good oral health or hygiene. An experienced head and neck clinician selected lesion/area in each patient for spectral studies and recorded its visual imprint. In the majority of patients, measurements were taken from each of the suspicious lesions and adjoining tissues (approximately 1 cm within the lesion boundary) for comparison. Clinical trials were conducted at the outpatient clinic of the Regional Cancer Centre (RCC), Trivandrum, India, on obtaining approval from the Ethics Committee of RCC. After explaining the modalities of the study, written informed consent was obtained from each patient/volunteer prior to enrollment.

The oral cavity is the most assessable site of the human body and has been used by many research groups in their pilot studies. Even though the epithelium is stratified throughout the

oral cavity, the mucous membrane differs in morphology at different sites. This affects the emission, particularly from DST, LST, and VBL mucosa, where the papillary structure prevails. Therefore, control LIAF and DR spectra were measured from the oral cavity of healthy volunteers at 14 different anatomical locations. A pictorial representation of the human oral anatomy showing the different measurement locations is given elsewhere.²⁵

Before commencement of the spectral measurements, the patients/volunteers were directed to hold 0.9% saline solution in their mouth for 5 minutes to reduce the effects of recently consumed food. Since the punch biopsy forceps cover an area of around 3×4 mm and its placement accuracy is difficult to control, after allowing a margin, an area 6 mm in diameter was chosen for each target site. In cases in which the lesion was smaller in size, the target site was restricted and biopsy of the entire lesion was taken. From each target site, 15 sets of fluorescence spectra were recorded and the mean spectrum is used to arrive at a statistically significant representation of the fluorescence/reflectance of the target site.

Biopsies taken from the measurement sites were fixed in 10% normal formalin and sent for histopathological analysis. The prepared histology slides were classified by an experienced pathologist blinded to the fluorescence spectral results. In the case of healthy volunteers, visual inspection was carried out instead of biopsy. After classification, spectroscopic data were correlated with the histopathological findings. An Independent Student's *t*-test was performed on the fluorescence ratios F500/F635, F500/F705, and F500/F685 and the reflectance ratio R545/R575.

RESULTS

Laser-Induced Autofluorescence Spectral Features of Oral Mucosa. The LIAF spectra show a broad autofluorescence peak at 500 nm that is characteristic of all oral epithelial tissues. Figure 2 represents the mean *in vivo* LIAF spectra recorded from 14 anatomical sites of the oral cavity in 36 healthy volunteers, normalized to the intensity of the 500 nm autofluorescence peak. Since the mean fluorescence spectra from sites other than DST, LST, and VBL show almost similar features, these could be averaged and the mean used as a control for detecting malignancy at these sites. On the contrary, fluorescence was observed at 635, 685, and 705 nm in healthy DST, LST, and VBL tissues. Since these emissions are very prominent in DST tissues and the occurrence rate of malignancy in DST was predominant over that in LST and VBL, the present investigation focuses on detection of cancers affecting DST sites.

Figures 3 and 4 compare the mean normalized *in vivo* LIAF spectra of different tissue types (i.e., healthy, hyperplastic, dysplastic, and squamous cell carcinoma (SCC)), in the 11 aforementioned anatomical locations and in DST. As can be seen from Fig. 3, fluorescence intensities at 635, 685, and 705 nm increase with the grade of tissue abnormality and can serve as a first-hand indicator of the grade of tissues.²⁵

Interestingly, we noticed that for the healthy DST tissues, the porphyrin-like emission peaks in the red region at 635, 685, and 705 nm are as intense as those of abnormal sites and even more intense than emission peaks of SCC. Therefore, LIAF could not be exploited as a tool for grading of DST tissues. Nevertheless, it could be noted that the emission intensity from abnormal DST tissues varies according to the grade of tissue

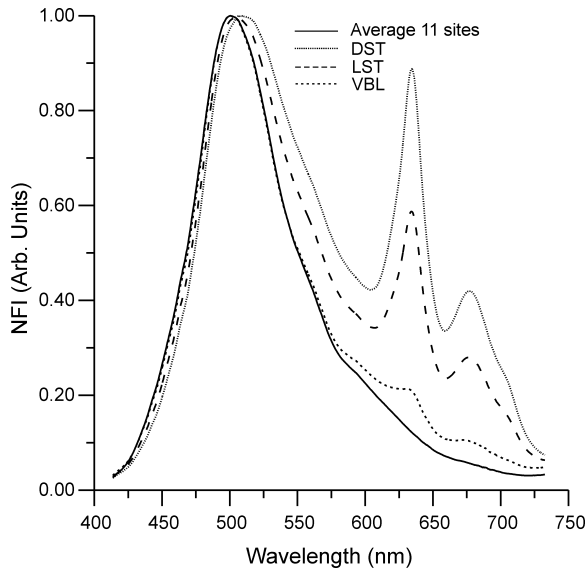


FIG. 2. Mean laser-induced autofluorescence (LIAF) spectra from the dorsal side of tongue (DST), lateral side of tongue (LST), and vermillion border of the lip (VBL) normalized to the autofluorescence intensity at 500 nm and compared with the mean spectrum from all 11 other sites of the oral cavity. DST, LST, and VBL spectra represent the mean of 15 measurements each in 36 volunteers, whereas the average normal spectrum relates to the mean of 15 measurements each at 11 sites in these volunteers. NFI stands for normalized fluorescence intensity.

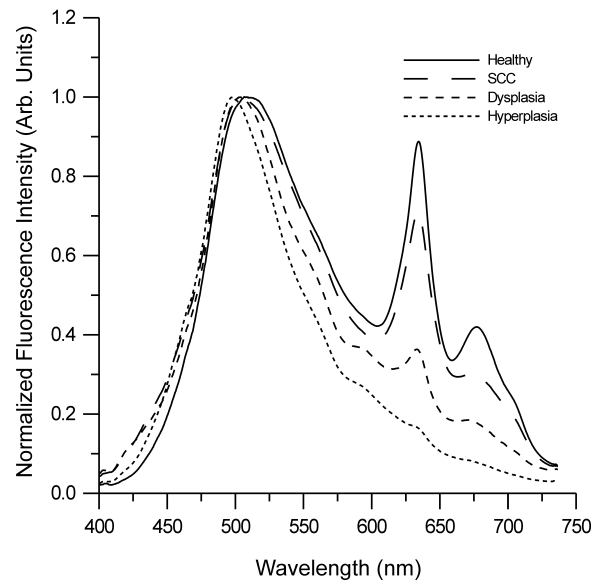


FIG. 4. Mean LIAF spectra from different grades of DST tissues from 30 sites in 16 patients and 36 healthy volunteers, normalized to the autofluorescence intensity at 500 nm. Healthy spectrum is the average of 36×15 measurements, hyperplastic spectrum is the average of 7×15 measurements, dysplastic spectrum is the average of 10×15 measurements, and SCC spectrum is the average of 13×15 measurements.

abnormality, as reported for buccal sites and other sites within the oral cavity.²⁵

Diffuse Reflection Spectral Features of Oral Mucosa.

Histopathological analysis of biopsy samples from oral mucosa adjoining malignant sites in patients that were considered to be normal often showed varying degrees of epithelial dysplasia

and hyperplasia. Therefore, such spectra could not be considered as representative of normal/healthy conditions. In order to overcome this, DR spectra were also measured from the oral cavity of healthy volunteers.²⁹ The mean DR spectrum of DST is used to represent normal/healthy tissues in this study.

The DR spectra of healthy and abnormal DST tissues show dips at 420, 545, and 575 nm due to oxygenated hemoglobin absorption.²⁹ Substantial variation in the *in vivo* DR spectral intensities were also observed between SCC, dysplasia, hyperplasia, and healthy DST mucosa. Figure 5 shows the

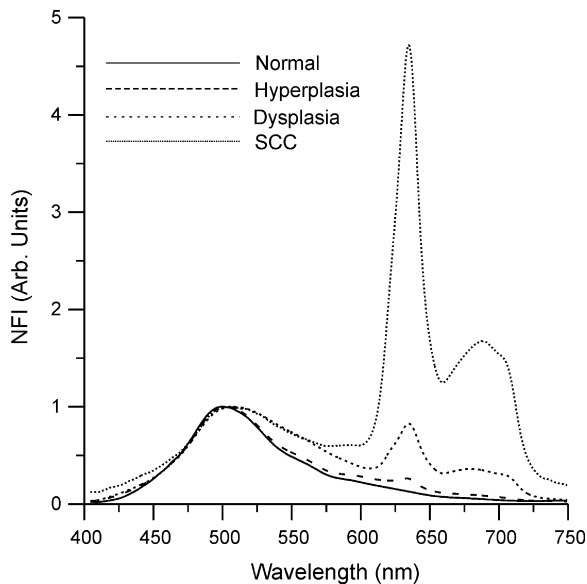


FIG. 3. LIAF emission from different types of oral mucosa from 40 sites in 20 patients and the mean spectra from 11 sites (other than DST, LST, and VBL) in 36 healthy volunteers, normalized to autofluorescence emission at 500 nm. Normal spectrum represents the average of 36×15 measurements in 11 sites, whereas spectra from the hyperplastic and dysplastic lesions are the mean of 9×15 measurements and the SCC lesion spectrum is the mean of 18×15 measurements.

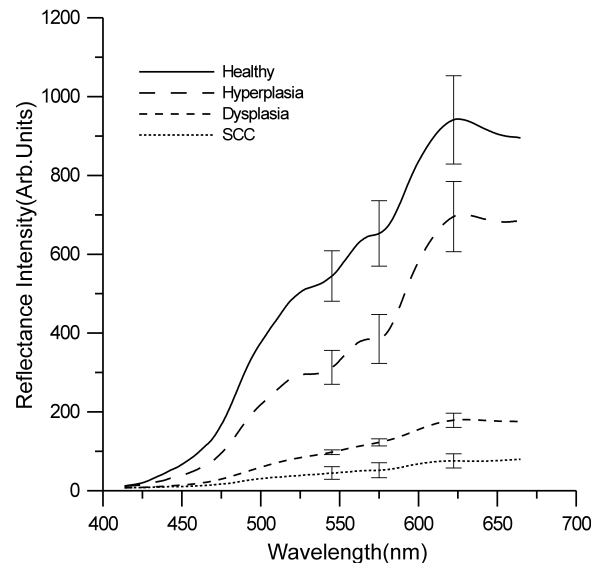


FIG. 5. Mean DR spectra from different grades of DST tissues at 30 sites in 16 patients and 36 healthy volunteers. Healthy spectrum is the mean of 36×15 measurements, hyperplastic spectrum is the mean of 7×15 measurements, dysplastic spectrum is the mean of 10×15 measurements, and SCC spectrum is the mean of 13×15 measurements.

mean DR spectra from squamous epithelium of DST in healthy volunteers and from 30 sites in 16 patients with varying grades of abnormality. As compared to healthy spectra, the oxygenated hemoglobin absorption dips at 545 and 575 nm were less prominent in abnormal lesions. The diffuse reflectance of malignant and premalignant lesions is lower and varies according to the grade of malignancy owing to increased absorption associated with changes in tissue morphology, in homogeneities, and break in the biosynthetic heme pathway.²⁹

DISCUSSION

Laser-Induced Autofluorescence Spectral Features of Oral Mucosa. Many research groups have reported that the broad autofluorescence around 500 nm is due to emission from endogenous fluorophores, such as nicotinamide adenine dinucleotide hydrogenase (NADH) and flavin adenine dinucleotide (FAD), collagen, elastin, and amino acids and the emissions at 635 and 705 nm from enhanced PpIX presence in the premalignant and malignant tissues,^{30–34} whereas the prominent peak around 685 nm in SCC tissues that appears between the PpIX emission peaks could be attributed to the accumulation of endogenous fluorophore corprophyrin III, which is a precursor of PpIX in the heme synthesis.^{25,35}

As can be seen from Fig. 2, porphyrin emissions in the red region are present particularly in healthy DST mucosa as compared to the other oral anatomical sites of healthy subjects. At these 11 anatomical sites it was observed that the 635 and 705 nm emissions appear and dominate the spectra as the tissue abnormality increases (Fig. 3) and serve as indicators of the grade of malignancy.²⁵ In contrast, the porphyrin-like emission observed for healthy DST tissues might have originated from bacterial colonization within the lingual papillary structure of these tissues, as proposed earlier (Fig. 4).²⁵ The possibility for deposition and retention of food particles in histological structures of DST is enormous, making these fertile grounds for bacterial colonization.³⁴ We observe that the presence of these abnormal peaks in healthy tissues could lead to erroneous diagnostic results as these could be marked as abnormal. However, an important and interesting point to be noted here is that in abnormal tissues of DST the intensity of the porphyrin peaks varied according to tissue abnormality with a minimum in hyperplasia and maximum in SCC tissues (Fig. 4), as observed in other anatomical sites (Fig. 3). Hyperplastic, dysplastic, and malignant SCC lesions are usually associated with hyperkeratotic layers. In the case of abnormal tissues of DST, such hyperkeratotic layers developed during abnormality over the papillary structure make the tissue surface flat as in the case of other mucosa, where the probability for deposition of food particles and ensuing bacterial growth and colonization is much less.

Laser-Induced Autofluorescence Site-Specific Spectral Ratio Reference Standards for DST Mucosa. Earlier studies have shown that LIAF spectral intensity ratios are highly sensitive and specific to discriminate different mucosal variations and to screen early stages of tissue progression towards malignancy for all the anatomical sites other than DST, LST, and VBL.²⁵ As described by Rupananda et al.,²⁵ site-specific SRRS scatter plots for DST sites were drawn using the three spectral intensity ratios F500/F635, F500/F685, and F500/F705 from 30 sites in 16 patients, comprising hyperplasia, dysplasia, and SCC. To avoid erroneous diagnosis, the mean ratios from the DST sites of 36 healthy volunteers were

used as normal for comparison. The average fluorescence intensity ratios (F500/F635, F500/F705, and F500/F685) determined from the LIAF spectra of the study population along with the results of histology, visual impression, and spectral impression for each ratio are given in Table I. Here, spectral impression indicates the evaluated grade of the tissue under question, based on of LIAF and DRS techniques as explained below.

Figures 6a–6c show the standard reference scatter plots for the three autofluorescence intensity ratios, which discriminate between contiguous normal, hyperplastic, dysplastic, and malignant grades of DST tissues. Discrimination lines were drawn between contiguous normal–hyperplastic, hyperplastic–dysplastic, and dysplastic–malignant groups at values that correspond to the average ratio values of the respective groups, as described elsewhere.²⁵ Conversely, in the case of non-contiguous grades such as normal vs. dysplasia, normal vs. SCC, hyperplasia vs. SCC, and groups of dysplasia+SCC vs. hyperplasia+normal we have developed separate independent LIAF and DRS scatter plots (not shown), where the cut-off lines are drawn at the mean value of the respective groups.

Diagnostic Accuracies for Laser-Induced Autofluorescence Spectral Ratio Reference Standards of DST. The diagnostic accuracies including sensitivity, specificity, positive predictive values (PPV), and negative predictive values (NPV) were assessed by validation using the gold standard. Cut-off values in the reference scatter plots in Figs. 6a–6c of the autofluorescence intensity ratios (F500/F635, F500/F685, and F500/F705) were used in the determination of diagnostic accuracies given in Table II for discriminating contiguous grades, i.e., normal/healthy tissues from hyperplastic, hyperplastic from dysplastic, and dysplastic from SCC lesions for all 30 DST sites in 16 patients. With the cut-off at 5.06, a sensitivity of 90% and specificity of 86% was obtained for discrimination of dysplastic and hyperplastic lesions using the F500/F635 ratio, with a PPV and NPV of 0.90 and 0.86, respectively. In the same plot, a cut-off line drawn at 2.77 discriminates premalignant dysplastic tissues from malignant SCC with a sensitivity of 85% and specificity of 90%, with PPV and NPV of 0.92 and 0.82, respectively. Using the information provided by the three SRRS plots together, a sensitivity of 93% and specificity of 72% with a PPV of 0.83 and NPV of 0.89 were achieved in distinguishing dysplastic from hyperplasia, whereas dysplasias could be discriminated from SCC with a sensitivity of 86% and specificity of 83%, with a PPV and NPV of 0.75 and 0.72, respectively.

Nevertheless, these figures are lower than the diagnostic accuracies attained for other anatomical sites using LIAF-SRRS in an earlier study²⁵ in which a sensitivity of 89% and specificity of 100% was achieved in distinguishing benign hyperplastic tissues from premalignant dysplastic mucosa, with a PPV and NPV of 0.98 and 1.0, respectively. In the past, many researchers have reported very low specificities with high sensitivities in detecting abnormal tissues in the oral cavity while using blue light to excite endogenous porphyrin fluorescence.^{8,26,27} We believe that these lower specificities might have been due to the inclusion of tongue tissues in their algorithms, where the possibility of false positives is too high to affect the overall diagnostic capability of the detection technique. It is to be noted that in all three discrimination scatter plots (Figs. 6a–6c) for DST, most of the normal tissue values occupied the position meant for SCC, which means that

TABLE I. Comparison of spectral impressions achieved using the fluorescence intensity ratios (F500/F635, F500/F705, and F500/F685) and the DR ratio (R545/R575) of the patient population with corresponding histological and visual impressions for DST.^a

P#	Histological impression	Visual impression	R545/R575	Spectral impression	F500/F635	Spectral impression	F500/F705	Spectral impression	F500/F685	Spectral impression
1	SCC	Ulcerative growth	0.865	SCC	3.22	Dysplasia	5.43	SCC	2.57	SCC
	Dysplasia	Proliferative growth	0.843	Dysplasia	3.56	Dysplasia	8.45	Dysplasia	4.33	Dysplasia
2	SCC	Ulceroproliferative lesion	0.867	SCC	1.70	SCC	5.23	SCC	2.27	SCC
	Hyperplasia	Normal	0.789	Normal	4.12	Dysplasia	8.53	Dysplasia	7.37	Dysplasia
3	SCC	Lesion	0.876	SCC	0.57	SCC	1.51	SCC	1.27	SCC
	Dysplasia	Normal	0.822	Dysplasia	3.50	Dysplasia	8.97	Dysplasia	7.15	Dysplasia
4	SCC	Ulceroproliferative lesion	0.874	SCC	3.43	Dysplasia	7.87	Dysplasia	5.99	Dysplasia
	SCC	Proliferative growth	0.855	SCC	2.15	SCC	7.21	Dysplasia	2.20	SCC
5	Dysplasia	Verrucous carcinoma	0.815	Hyperplasia	2.37	SCC	8.04	Dysplasia	4.64	Dysplasia
	Dysplasia	Verrucous carcinoma	0.832	Dysplasia	4.54	Dysplasia	17.81	Hyperplasia	5.66	Dysplasia
6	SCC	Lesion	0.856	SCC	1.07	SCC	2.91	SCC	2.39	SCC
	Hyperplasia	Normal	0.812	Hyperplasia	8.48	Hyperplasia	36.16	Hyperplasia	9.56	Hyperplasia
7	SCC	Lesion	0.859	SCC	2.24	SCC	8.26	Dysplasia	3.99	SCC
	SCC	Superficial growth	0.880	SCC	1.25	SCC	2.86	SCC	4.40	Dysplasia
8	SCC	Superficial growth	0.876	SCC	1.25	SCC	2.86	SCC	3.86	SCC
	Dysplasia	Leukoplakia	0.847	SCC	3.22	Dysplasia	5.43	SCC	3.75	SCC
9	SCC	Homogeneous leukoplakia	0.840	Dysplasia	2.50	SCC	8.88	Dysplasia	5.21	Dysplasia
	Dysplasia	Erythroplakia	0.835	Dysplasia	2.97	Dysplasia	5.31	SCC	4.37	Dysplasia
10	Hyperplasia	Normal	0.836	Dysplasia	6.33	Hyperplasia	19.69	Hyperplasia	14.45	Dysplasia
	SCC	Homogeneous leukoplakia	0.852	SCC	2.37	SCC	8.16	Dysplasia	2.19	SCC
11	SCC	Lesion	0.840	Dysplasia	2.24	SCC	8.26	Dysplasia	1.92	SCC
	Hyperplasia	Normal	0.817	Hyperplasia	6.75	Hyperplasia	27.92	Hyperplasia	18.60	Hyperplasia
12	Dysplasia	Superficial growth	0.840	Dysplasia	2.88	Dysplasia	7.26	Dysplasia	6.87	Dysplasia
13	SCC	Ulceroproliferative growth	0.869	SCC	1.18	SCC	4.45	SCC	2.72	SCC
14	Dysplasia	Proliferative lesion	0.852	Dysplasia	3.6	Dysplasia	8.20	Dysplasia	6.60	Dysplasia
	Dysplasia	Normal	0.841	Dysplasia	4.31	Dysplasia	7.70	Dysplasia	7.70	Dysplasia
15	Hyperplasia	Traumatic ulcer	0.809	Hyperplasia	6.4	Hyperplasia	13.40	Dysplasia	13.40	Hyperplasia
	Hyperplasia	Normal	0.799	Hyperplasia	5.67	Hyperplasia	14.50	Hyperplasia	14.50	Hyperplasia
16	Dysplasia	Leukoplakia	0.832	Dysplasia	5.2	Hyperplasia	11.20	Dysplasia	11.20	Dysplasia
	Hyperplasia	Traumatic ulcer	0.820	Dysplasia	7.79	Hyperplasia	8.44	Dysplasia	8.44	Dysplasia

^a P#: Patient number; misclassified spectral diagnosis are in bold.

all true negative values were being wrongly identified as true positives. Again, poor diagnosis accuracies were observed in differentiation of non-contiguous tissue grades involving normal tissues, i.e., normal from dysplasia, normal from SCC, and a group of dysplasia+SCC from hyperplasia+normal. This indicates the incapability of LIAF-SRRS technique to differentiate normal DST oral mucosa from abnormal DST dysplasia and SCC. However, discrimination among the non-contiguous abnormal tissues was quite good, with relatively high accuracies. For example, DST hyperplastic tissues were well differentiated with a sensitivity of 89% and specificity of 100% with a PPV of 1 and NPV of 0.79 from the non-contiguous SCC grade tissues.

Diffuse Reflection Spectral Ratio Reference Standards in Tissue Grading of DST Mucosa. The mean diffuse reflection spectral intensity ratio (R545/R575) at the oxygenated hemoglobin absorption maxima was calculated at different DST sites having diverse tissue characteristics in the healthy and patient populations. The R545/R575 ratio is lowest for normal tissue and its increasing trend with higher grades of cancer points to the distinct possibility of using this ratio for tissue classification. The results of histopathological examination, visual impression by the clinician, and spectral impression based on scatter plots of the R545/R575 ratio are presented in Table I.

Figure 7 shows the site-specific SRRS scatter plot of the oxygenated hemoglobin ratio (R545/R575) on the same patient cohort derived from DRS for discriminating hyperplastic, dysplastic, and malignant DST tissues. Discrimination lines are

drawn between the normal–hyperplastic, hyperplastic–dysplastic, and dysplastic–SCC ratios at values that correspond to the average ratio value of the respective groups, as described earlier.²⁹

Contrary to the LIAF scatter plots (Figs. 6a–6c), the R545/R575 ratio for normal tissues in Fig. 7 occupies the designated positions without displacement to other groupings and the ratio values were found to increase according to the progression to higher grades of malignancy. The classification sensitivity, specificity, PPV, and NPV for discriminating each of these categories were determined based on the discrimination threshold values by validation with the gold standard, as described before.

Diagnostic Accuracies of Diffuse Reflection Spectral Ratio Reference Standards of DST. The sensitivity and specificity for discrimination of contiguous hyperplastic from normal tissues of DST using DRS-SRRS were 75% and 97%, respectively, with a positive predictive value of 0.86 and negative predictive value of 0.94 (Table II). However, for discriminating precancerous (dysplastic) DST tissues from hyperplastic tissues, a sensitivity of 90% and specificity of 86% was achieved, with a PPV of 0.90 and a NPV of 0.86. On the other hand, dysplastic lesions were distinguishable from SCC with a sensitivity of 86% and specificity of 94%, with a corresponding PPV of 0.75 and NPV of 0.97. Owing to the limited number of patients screened with abnormal DST, the sensitivities and specificities calculated could only be considered as relative.

As compared to LIAF-SRRS, the discrimination of non-

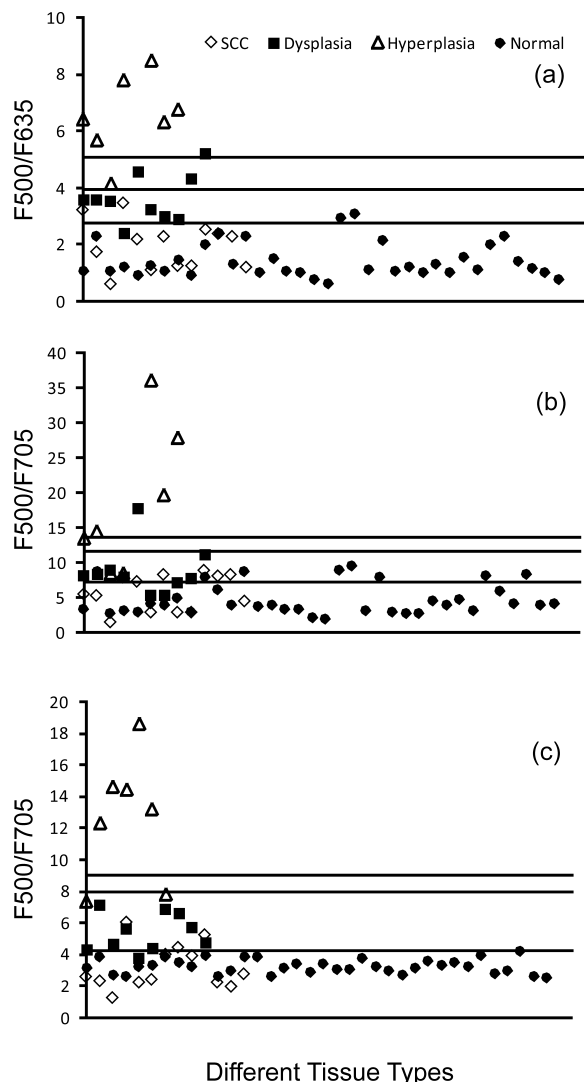


FIG. 6. Site-specific spectral ratio reference standard (SRRS) developed using the fluorescence intensity ratios: (a) F500/F635, (b) F500/F685, and (c) F500/F705 from the dorsal tongue in 36 healthy volunteers and from 30 sites in 16 patients.

contiguous DST tissue grades was better with DRS-SRRS. Based on the information provided by DRS-SRRS, a sensitivity and specificity of 100% with a PPV and NPV of 1.0 was achieved to distinguish non-contiguous normal from dysplastic

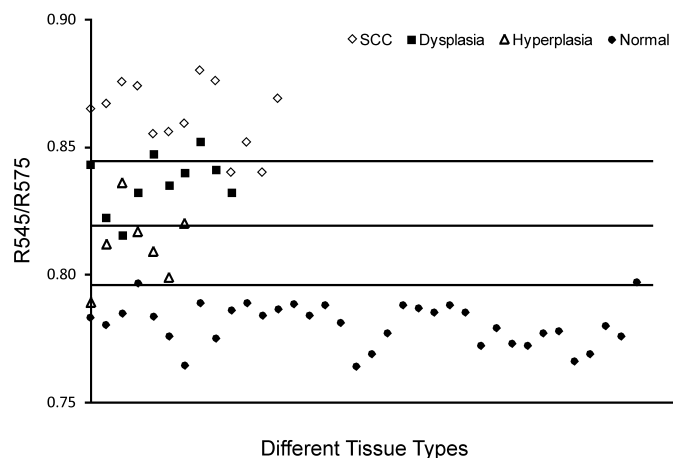


FIG. 7. Site-specific DR spectral ratio scatter plot developed for discriminating different DST tissues from 30 sites in 16 patients.

and SCC tissues, respectively, whereas, non-contiguous hyperplasias could be discriminated from SCC with a sensitivity and specificity of 100% and a PPV and NPV of 1 and 0.80, respectively.

Since the ratio values show a distinct increasing trend with increasing grades of abnormality (Fig. 7), discrimination between contiguous and non-contiguous tissue grades was possible with DRS-SRRS. In a previous study using LIAF-SRRS at anatomical sites other than DST, LST, and VBL, we have observed that the three fluorescence peak intensity ratios (F500/F635, F500/F705, and F500/F685) have a decreasing trend with increasing grades of tissue abnormality.²⁵ This led to very good diagnostic accuracies for discrimination of contiguous and non-contiguous tissue grades. However, in the present study, a similar decreasing trend was not observed in the LIAF ratios of DST tissues as most of the normal/healthy ratio values were occupying positions meant for SCC, leading to the poor diagnostic accuracies represented in Table II.

The average DRS ratio (R545/R575) and the corresponding spectral impression are also given in Table I along with the LIAF spectral ratios for comparison. Spectral impression of each site (Table I) is based on the spectral ratios of scatter plots shown in Fig. 6 and Fig. 7 and represents the evaluated grade of DST tissue under question, based on the discrimination scatter plots of LIAF and DRS ratios. Visually, it is not possible to differentiate between various tissue types; what a clinician can do at best is to discriminate between normal and

TABLE II. Comparison of sensitivities and specificities of different LIAF and DR ratios in discriminating different tissue types of DST *in vivo*. Corresponding PPV and NPV values are shown in parenthesis.

Diagnostic accuracies	Ratios	Normal vs. hyperplasia	Normal vs. dysplasia	Normal vs. SCC	Hyperplasia vs. dysplasia	Hyperplasia vs. SCC	Dysplasia vs. SCC	Dysplasia+SCC vs. normal+hyperplasia
Sensitivity (%) (PPV)	F500/F635	2(0.13)	3(0.1)	72(0.44)	90 (0.90)	93(1)	85(0.92)	29(0.65)
	F500/F685	5(0.25)	2(0.1)	32(0.62)	100(0.83)	87(1)	77(0.91)	36(0.87)
	F500/F705	5(0.25)	7 (0.2)	39(0.46)	90(0.75)	87(1)	62(0.80)	37(0.96)
	Together	4(0.21)	4(0.13)	60(0.51)	89(0.83)	89(1)	75(0.88)	34(0.83)
Specificity (%) (NPV)	R545/R575	75(0.86)	100(1)	100(1)	90(0.90)	100(1)	86(0.75)	96(0.96)
	F500/F635	0(0)	97(0.05)	62(0.25)	86(0.86)	100(0.88)	90(0.82)	50(0.18)
	F500/F685	0(0)	10(0.2)	80(0.50)	72(1.00)	100(0.75)	80(0.72)	72(0.18)
	F500/F705	0(0)	50(0.22)	38(0.28)	57(0.80)	100(0.75)	80(0.62)	88(0.16)
	Together	0(0)	53 (0.1)	54(0.34)	72(0.89)	100(0.79)	83(0.72)	70(0.17)
	R545/R575	97(0.94)	100(1)	100(1)	86(0.86)	100(0.80)	94(0.97)	98(0.98)

TABLE III. Comparison of ROC-AUCs for LIAF and DRS ratios for discerning different DST tissues types.^a

Spectral intensity ratios	ROC-AUC							Overall accuracy for each ratio
	Normal vs. hyperplasia	Normal vs. dysplasia	Normal vs. SCC	Hyperplasia vs. dysplasia	Hyperplasia vs. SCC	Dysplasia vs. SCC	Dysplasia+SCC vs. normal+hyperplasia	
F500/F635	0.000	0.017	0.293	0.957	1.000	0.927	0.320	0.502
F500/F705	0.028	0.147	0.419	0.871	0.978	0.760	0.403	0.515
F500/F685	0.000	0.022	0.610	0.864	1.000	0.870	0.472	0.405
Mean F-ratio	0.009	0.062	0.441	0.897	0.993	0.852	0.398	0.521
R545/R575	0.988	1.000	1.000	0.900	1.000	0.927	0.993	0.970

^a ROC-AUC: Receiver operation characteristic-area under curve.

abnormal mucosa. However, the results of the present study show that those adjoining (margin) lesions diagnosed histologically as hyperplasia (Patients # 6, 10, 11, and 15, in Table I) and dysplasia (Patients #3 and 14) were misclassified by the clinician as normal. This shows that abnormal tissues need not necessarily provide a correct visual impression to a clinician although abnormality may be present microscopically. Further, it was noticed that the DRS scatter plot categorizes most of these sites accurately as abnormal. In one case (Patient #10), the tissue that was identified clinically as homogeneous leukoplakia was found to be SCC upon histological analysis and also with the spectral impression based on SRRS of the R545/R575 ratio and with the LIAF SRRS ratios (F500/F635, F500/F685, and F500/F705).

As can be seen from Table I, among the LIAF scatter plots developed, the F500/F705 ratio scatter plot had the maximum number of misclassifications (12 out of 30), while the F500/F635 ratio scatter plot produced the best classification (6 out of 30). In other words, LIAF-SRRS has produced an overall classification accuracy of 8 out of 30 in the patient population. In comparison, the R545/R575 SRRS produced a classification accuracy of 7 out of 30 in the patient population. Also, in the DRS scatter plot shown in Fig. 7, misclassification between normal and hyperplasia occurred in only 3 out of 43 cases. This shows that the DRS R545/R575 ratio scatter plot provides fairly good accuracy in discriminating between normal and hyperplastic tissues *in vivo*.

Comparison of Laser-Induced Autofluorescence and Diffuse Reflection Spectroscopy Using Receiver Operating Characteristic Curve Analysis. In order to check the adequacy of LIAF and DR methodologies in discriminating different DST tissue types, receiver operating characteristic (ROC)-curve analysis³⁶⁻³⁸ was performed on the three LIAF intensity ratios and the DR oxygenated hemoglobin ratio using SPSS (Version 10) software. SPSS automatically calculates the sensitivity and specificity of given input ratio values and plots the ROC curves, with sensitivity values against the values of 1-specificity for a default confidence interval of 95%. For both LIAF and DRS, the classification of these lesions was successful with very good values of ROC-AUC. Table III shows the ROC-curve plotted using sensitivity and specificity values attained for the LIAF ratios (F500/F635, F500/F685, and F500/F705) and the DR HbO₂ ratio (R545/R575) to discriminate different grades of oral mucosa.

As mentioned earlier, visual examinations by clinicians have the potential to identify lesions as normal (hyperplasia+healthy) or abnormal (dysplasia+SCC), but not individually. The majority of contemporary optical studies have been undertaken to distinguish normal (a group of healthy and hyperplasia/

benign) from abnormal (a group of dysplastic and malignant) tissues³⁹⁻⁴² or dysplastic from malignant lesions^{39,42,43} or normal from malignant lesions^{39,44,45} or cancerous and high grade dysplasia from low grade, benign, and normal.⁴⁶ However, as of now, most of the studies are being focused on the search for an optical modality that could be a noninvasive alternative to histopathology by providing grading, even intra-grading of dysplasia (mild, moderate, and severe) and SCC (well differentiated, moderately differentiated, and poorly differentiated) or at least an adjunct to the clinicians to locate the most abnormal portion of the lesion under question for biopsy. This can possibly lead to elimination of the subjective nature of histopathology, due to its dependence on clinically guided biopsy.

These facts indicate that the real challenge for an alternate diagnostic system is to detect early tissue transformations, i.e., the ability to discriminate contiguous tissue grades, particularly premalignant lesions from clinically similar hyperplasias. As a consequence, the relevant question is not whether the suspicious tissue or lesion is normal or abnormal, because it has already been established as abnormal from its appearance by the clinician. The relevant question here should instead be whether the visible tissue alterations are of a benign or premalignant nature, and the modality used would facilitate detection of cancer in its incipient stage. The answer to this question is crucial for classification of visible lesions and in treatment planning. Based on this clinical rationale, we believe that the significance of any technique lies in the ability to differentiate between contiguous grades of oral tissues, i.e., normal/healthy, hyperplasia or benign, dysplasia, and SCC. However, to maintain consistency with Table II we have calculated ROC-AUCs for different tissue groups other than these four contiguous grades, and these are presented in Table III.

In the discrimination of hyperplastic from dysplastic lesions using the LIAF ratios F500/F635 and F500/F705, the ROC-AUC were 0.957 and 0.870, respectively, while for the F500/F685 ratio it was 0.864. The three LIAF ratios together have a ROC-AUC of 0.897, whereas for the DR ratio (R545/R575) the ROC-AUC was 0.9 for discriminating the same set of DST tissues.

In another study, using a different combination of normalization methods and classifiers, de Veld et al. (2005)²⁴ obtained a ROC-AUC <0.65 in differentiating hyperplastic tissues from dysplastic tissues, for different excitation wavelengths. In the same study, applying the same procedure to DRS spectra, they reported a lower ROC-AUC in the 0.70 to 0.77 range. These values are well below the values achieved in the current study using LIAF and DRS spectral ratios.

As far as the present study is concerned, the three LIAF ratios jointly gave an overall ROC-AUC of 0.521 in differentiating between different tissues types of DST (i.e., normal–hyperplastic, normal–dysplastic, normal–SCC, hyperplastic–SCC, hyperplastic–dysplastic, dysplastic–SCC, and a group of normal+hyperplastic–dysplasia+SCC), whereas the DR ratio gave a better accuracy of 0.970. Besides, for distinguishing healthy tissues from hyperplastic tissues, where the LIAF ratios are useless owing to the very poor mean ROC-AUC of 0.009, the DR ratio gave a very good discrimination accuracy of 0.988. Thus, the ROC-curve analysis has shown DRS-SRRS to be a better diagnostic tool as compared to LIAF-SRRS in distinguishing different DST tissues, not only in terms of its better diagnostic accuracies but in its capability to discriminate between different malignant grades.

CONCLUSION

The comparative critique between LIAF and DRS has shown that cancers affecting the dorsal side of tongue are always difficult to diagnose and grade using tissue autofluorescence signatures owing to the presence of porphyrin-like emission in normal tissues. Even though LIAF-SRRS can distinguish between different abnormal DST tissues, the diagnostic accuracies are low. The misclassification of a large number of normal DST tissues as SCC shows the frailty of LIAF in grading of DST cancer. This predicament was resolved to a great extent by using the SRRS of oxygenated hemoglobin absorption ratio (R545/R575) from the diffuse reflection spectrum in a clinical experiment on the same patient cohort, where the majority of DST tissue types were discriminated from one another with good diagnostic accuracies. Further, from the available results, it can be shown that DRS-SRRS differentiates early stages of contiguous DST tissue transformations with high accuracies; for example, hyperplastic (benign) tissues could be distinguished from normal with a sensitivity of 75% and specificity of 97%, whereas for distinguishing hyperplastic from dysplastic (pre-malignant) tissues, which is a major challenge for the researchers, the DRS-SRRS gave an improved sensitivity of 90% and specificity of 86%. Also, for differentiating various non-contiguous DST grades involving normal tissues, where LIAF-SRRS was not successful, DRS-SRRS has given very good diagnostic accuracies. Further, the observed overall ROC-AUC (mean accuracy in differentiating the different tissue types) of 0.970 for the DRS ratio is superior to the ROC-AUC of 0.521 obtained for LIAF. This shows the authenticity and potential of the DRS ratio in discriminating different tongue mucosa and calls for a prospective study in a larger patient group.

Even though, there is no rule of thumb regarding study population, we feel the basic constraint of this study was with respect to the patient population, especially as the study is site specific and lesions were divided into different categories for classification. Again, as described earlier, the major limitation associated with point monitoring is that it takes a lot of time to scan an entire lesion point by point, which could be overcome with the use of multispectral imaging systems based on intensified CCD (ICCD) or EMCCD cameras that can gather fluorescence/reflection images of the entire lesion in a short time. Again, it is vital to explore the possibilities to differentiate between different grades of SCC that are not investigated under this study.

Based on our findings it can be concluded that the

information provided by noninvasive DR spectroscopy along with suitable analytical methods has immense potential to diagnose oral tongue cancer in its early stages. This study has clearly shown that the DR methodology that uses oxygenated hemoglobin absorption features could act as an adjunct to LIAF and other techniques for clinical detection of tongue cancer, and the possibility of speedy diagnosis facilitates early follow-up decisions, ensuing in treatment or surgery. Thus, the DR ratio technique by virtue of its low cost and high sensitivity and specificity has the potential to become a viable alternative for *in vivo* tongue cancer screening of larger populations through community centers.

ACKNOWLEDGMENTS

This project was carried out with grants from the Department of Science and Technology (DST), Govt. of India, and the CESS Plan-223 project. The authors are thankful to the Research Council (RC) of CESS and the Institutional Review Board and Ethics Committee of RCC for their encouragement and support. R.J.M. acknowledges the DST and CSIR, New Delhi, for his research fellowships. We are grateful to all the healthy volunteers and patients for their willingness to take part in the clinical trials and also to Ms. Sara Thomas Shiny for her support during clinical trials.

1. B. W. Neville, D. D. Damm, C. M. Allen, and J. E. Bouquot, "Epithelial Pathology", in *Oral Maxillofacial Pathology* (W. B. Saunders, Philadelphia, 1995), pp. 259–321.
2. J. Forlay, D. M. Parking, and P. Pissani, *Globscan 2002: Cancer Incidence Mortality and Prevalence Worldwide* (Lyon IARC publication, 2007).
3. D. C. G. de Veld, M. Skurichina, M. J. Witjes, R. P. W. Duin, H. J. C. M. Sterenberg, and J. L. N. Roodenburg, *J. Biomed. Opt.* **9**, 940 (2004).
4. T. Wu, J. Y. Qu, T. H. Cheung, W.-K. K. Lo, and M.-Y. Yu, *Opt. Exp.* **11**, 291 (2003).
5. W. C. Lin, S. A. Toms, M. Johnson, E. D. Jansen, and J. A. Mahadevan, *Photochem. Photobiol.* **73**, 396 (2001).
6. C. Eker, R. Rydell, K. Svanberg, and S. Andersson-Engels, *Lasers. Surg. Med.* **28**, 259 (2001).
7. J. Y. Qu, P. Wing, Z. Huang, D. Kwong, J. Sham, L. S. Lung, H. W. Kuen, and W. I. Wei, *Lasers. Surg. Med.* **26**, 432 (2000).
8. C. S. Betz, M. Mehlmann, K. Rick, H. Stepp, G. Grevers, R. Baumgartner, and A. Leunig, *Lasers Surg. Med.* **25**, 323 (1999).
9. G. A. Wagnieres, W. Star, and B. C. Wilson, *Photochem. Photobiol.* **68**, 603 (1998).
10. S. P. Schantz, V. Kolli, H. E. Savage, G. Yu, J. P. Shah, D. E. Harris, A. Katz, R. R. Alfano, and A. G. Huvos, *Clin. Cancer. Res.* **4**, 1177 (1998).
11. R. Richards-Kortum and E. Sevick-Muraca, *Ann. Rev. Phys. Chem.* **7**, 555 (1996).
12. N. Ramanujam, M. F. Mitchell, A. Mahadevan, S. Warren, S. Thomsen, E. Silva, and R. Richards-Kortum, *Proc. Natl. Acad. Sci. U.S.A.* **91**, 10193 (1994).
13. K. T. Schomacker, J. K. Fusoli, C. C. Compton, T. J. Flotte, J. M. Richter, N. S. Nishioka, and T. F. Deutsch, *Lasers Surg. Med.* **12**, 63 (1992).
14. G. F. Rubino and L. Rasetti, *Panminerva. Med.* **8**, 290 (1966).
15. M. Kondo, N. Hirota, T. Takaoka, and M. Kajiwara, *Cell. Biol. Toxicol.* **9**, 95 (1993).
16. K. Soklov, R. Drezek, K. Gossage, and R. Richards-Kortum, *Opt. Exp.* **5**, 302 (1999).
17. U. Utzinger, M. Brewer, E. Silva, D. Gershenson, R. C. Blast, Jr., M. Follen, and R. Richards-Kortum, *Lasers. Surg. Med.* **28**, 56 (2001).
18. G. Zonios, L. T. Perelmann, V. Backmann, R. Manoharan, M. Fitzmaurice, J. V. Dam, and M. S. Feld, *Appl. Opt.* **38**, 6628 (1999).
19. I. Georgakoudi, B. C. Jacobson, M. G. Muller, E. E. Sheets, K. Badizadegan, D. L. Carr-Locke, C. P. Crum, C. W. Boone, R. R. Dasari, J. V. Dam, and M. S. Feld, *J. Cancer. Res.* **62**, 682 (2002).
20. K. R. Diamond, T. J. Farrell, and M. S. Patterson, *Phys. Med. Biol.* **48**, 4135 (2003).
21. M. G. Muller, I. Georgakoudi, Q. Zhang, J. Wu, and M. S. Feld, *Appl. Opt.* **40**, 4633 (2001).
22. Q. Zang, M. G. Muller, J. Wu, and M. S. Feld, *Opt. Lett.* **25**, 1451 (2000).
23. J. M. C. C. Coremans, C. Ince, H. A. Bruining, and J. Puppels, *Biophys. J.* **72**, 1849 (1997).
24. D. C. G. de Veld, M. Skurichina, M. J. H. Witjes, R. P. W. Duin, H. J. C.

- M. Sterenborg, and J. L. N. Roodenburg, *Lasers. Surg. Med.* **36**, 356 (2005).
25. J. M. Rupananda, N. Subhash, S. T. Shiny, R. Rejnish Kumar, M. Anitha, M. Jaiprakash, and S. Paul, *Cancer* **112**, 1512 (2008).
 26. J. K. Dhiranga, D. F. Perrault, K. McMillan, E. E. Rebeiz, S. Kabani, R. Manoharan, I. Itzkan, M. S. Feld, and S. M. Shapshay, *Arch. Otolaryngol. Head. Neck. Surg.* **122**, 1181 (1996).
 27. A. Gillenwater, R. Jacob, R. Ganeshappa, B. Kemp, A. K. El-Naggar, J. L. Palmer, G. Clayman, M. F. Mitchell, and R. Richards-Kortum, *Arch. Otolaryngol. Head. Neck. Surg.* **124**, 1251 (1998).
 28. N. Subhash, J. M. Rupananda, S. T. Shiny, M. Anitha, M. Jaiprakash, and S. Paul, *J. Biomed. Opt.* **11**, 014018 (2006).
 29. J. M. Rupananda, S. T. Shiny, M. Anitha, S. Paul, M. Jayaprakash, and N. Subhash, *J. Biomed. Opt.* **13**, 041306 (2008).
 30. R. S. DaCosta, H. Anderson, and B. Wilson, *Photochem. Photobiol.* **78**, 384 (2003).
 31. R. Drezek, K. Sokolov, U. Utzinger, I. Boiko, A. Malpica, M. Follen, and R. Richards-Kortum, *J. Biomed. Opt.* **6**, 385 (2001).
 32. D. R. Ingrams, J. K. Dhingra, K. Roy, D. F. Perrault, I. D. Bottrill, S. Kabani, E. E. Rebeiz, M. M. Pankratov, S. M. Shapshay, R. Manoharan, I. Itzkan, and M. S. Feld, *Head Neck* **19**, 27 (1997).
 33. R. Richards-Kortum and E. Sevick-Muraca, *Annu. Rev. Phys. Chem.* **47**, 555 (1996).
 34. D. C. G. de Veld, S. Marina, M. J. H. Witijes, R. P. W. Duin, D. J. C. M. Sterenborg, W. M. Star, and J. L. N. Roodenburg, *Lasers. Surg. Med.* **23**, 367 (2003).
 35. K. T. Moesta, E. Bernd, H. Tim, N. Dirk, N. Christian, E. H. Wolfgang, K. P. Ravindra, J. D. Thomas, R. Herbert, and M. S. Peter, *Cancer Res.* **61**, 991 (2001).
 36. M. H. Zweig and G. Campbell, *Clin. Chem.* **39**, 561 (1993).
 37. P. F. Griner, R. J. Mayewski, A. I. Mushlin, and P. Greenland, *Annal. Int. Med.* **94**, 555 (1981).
 38. C. E. Metz, *Semin. Nucl. Med.* **8**, 283 (1978).
 39. M. G. Muller, T. A. Valdez, I. Georgakoudi, V. Backman, C. Kabani, N. Laver, Z. Wang, C. W. Boone, R. R. Dasari, S. M. Shapshay, and M. S. Feld, *Cancer* **97**, 1681 (2003).
 40. Z. Volynskaya, A. S. Haka, K. L. Bechtel, M. Fitzmaurice, R. Shenk, N. Wang, J. Nazemi, R. R. Dasari, and M. S. Feld, *J. Biomed. Opt.* **13**, 024012 (2008).
 41. C. Zhu, G. M. Palmer, T. M. Breslin, J. Harter, and N. Ramanujam, *Lasers Surg. Med.* **38**, 714 (2006).
 42. J. R. Mourant, I. J. Bigio, J. Boyer, R. L. Conn, T. Johnson, and T. Shimada, *Lasers Surg. Med.* **17**, 350 (1995).
 43. D. C. G. de Veld, S. Marina, M. J. H. Witijes, R. P. W. Duin, H. J. C. M. Sterenborg, and J. L. N. Roodenburg, *Lasers Surg. Med.* **36**, 356 (2005).
 44. D. M. Anjan Dhar, K. S. Johnson, M. R. Novelli, S. G. Bown, I. J. Bigio, L. B. Lovat, and S. L. Bloom, *Gastroint. Endosc.* **63**, 257 (2006).
 45. I. J. Bigio, S. G. Bown, G. Briggs, C. Kelley, S. Lakshmi, D. Pickard, P. M. Ripley, I. G. Rose, and C. Saunders, *J. Biomed. Opt.* **5**, 221 (2000).
 46. S. Y. Park, M. Follen, A. Milbourne, H. Rhodes, A. Malpica, N. MacKinnon, C. MacAulay, M. K. Markey, and R. Richards-Kortum, *J. Biomed. Opt.* **13**, 014029 (2008).